Research Article Vol. 62, No. 17 / 10 June 2023 / Applied Optics 4571

applied optics

Method to construct the initial structure of optical systems based on full-field aberration correction

Xianxing Chen,[1,2] Xu Zhang,[1,2] Zhiqiang Su,[1] Jie Yu,[1,3] and Liping Wang[1,3,*]

[1]Changchun Institute of Optics, Fine Mechanics and Physics, Chinese Academy of Sciences, Changchun, Jilin 130033, China
[2]University of Chinese Academy of Sciences, Beijing 100039, China
[3]State Key Laboratory of Applied Optics, Changchun, Jilin 130033, China
*wlp8121@126.com

Received 2 March 2023; revised 17 April 2023; accepted 22 April 2023; posted 24 April 2023; published 6 June 2023

To meet full-field image quality requirements for extremely low aberration optical systems, an initial structure construction method for reflective optical systems based on full-field aberration correction is proposed. The aberration of the full field is used as the main evaluation criterion in this method. A multi-field evaluation function is established using the aberration values of multiple characteristic field points to represent the full-field imaging quality, and spatial ray tracing is introduced to constrain the optical system structure. Multi-objective optimization of the evaluation function is performed using a combinatorial nondominated sorting and metaheuristics algorithm; an initial optical system with a reasonable structure and corrected third-order aberrations over the full field is subsequently obtained. After optimization, an extreme ultraviolet lithography objective with a numerical aperture of 0.33 and root-mean-square wavefront error of 0.128 nm (1/105λ, λ = 13.5 nm) is obtained.

https://doi.org/10.1364/AO.488647

1. INTRODUCTION

Because of the presence of aberrations, the imaging performance of an optical system will typically decrease when the object field-of-view (FOV) increases, which leads to considerable degradation of the image resolution in the edge field when compared with the center field. This degradation is unacceptable in extreme ultraviolet lithography (EUVL) projection optics that have high image quality requirements. To achieve high-resolution projection imaging, the lithographic objective is required to provide extremely high image quality over the full-field range, and the full-field composite aberration is better than 1/50λ root-mean-square (RMS) [1]. However, EUVL projection optics has a relatively wide FOV; the process of controlling the extremely low aberrations over the full field becomes extremely difficult, and it is then difficult to obtain a projection optical system that meets the full-field aberration requirements. Additionally, because of the number of system optimization variables and severe coupling of the constraint limits, the design results obtained via optical design software optimization are usually local solutions that are close to the initial structure, highly susceptible to local minima, and have major limitations. If the third-order aberration of the initial constructed structure has been corrected over the full field, it will greatly reduce the difficulty of system optimization for extremely low aberration over the full field. Therefore, to solve the problem of designing an EUVL projection optics that must satisfy the requirement for extremely low aberration over the full field, the addition of the condition of full-field aberration correction to the initial structure's construction process is a feasible option.

In recent years, many optical designers have proposed a series of methods for designing the initial structures of reflective optical systems; these methods mainly included the $Y-\bar{Y}$ design method, the novel design method, the differential equation design method, the grouping design method, a method of a combination of spatial ray tracing and aberration correction, the discrete points fitting method [2], and an automatic design method based on the coaxial Seidel aberration theory [3]. The $Y-\bar{Y}$ design method, which is also known as the Delano chart design method [4], was applied by Sasian in 2000 to the design of four-mirror EUVL objectives [5]. A novel design method was proposed by Marinescu of Delft University [6]. For multi-mirror optical systems, the calculation process of the $Y-\bar{Y}$ design method will then become highly complex, and the novel design method does not guarantee that an unobstructed system can be obtained. Additionally, neither method can be used for the initial structural design of aspheric systems. To find an initial structure for a reflective optical system with aspheric surfaces accurately, a differential equation design method for EUVL objectives was proposed by Wang and Shealy [7,8]. However, the method requires a large number of quantities about the system structure to be known, and it does not have universal design applicability. In 2013, Li's team at Beijing Institute of Technology applied the group design method to design an EUVL projection optics structure [9]. They divided the desired

six-mirror EUVL objective system into three groups—the object-side mirror group, the image-side mirror group, and the intermediate mirror group— determined the structural parameters for each mirror group based on spatial ray tracing for constraint control, and then stitched the three mirror groups together using the principle of pupil matching. This method not only simplifies the difficulty of the multi-mirror system design, but also allows the spatial structure of the system to be constrained by introducing spatial ray tracing. However, the above design methods for the initial structure of reflective optical systems are based on the first-order parameters of a single field, which do not provide a good starting point for the problem of aberration correction in the subsequent optimization process. To solve the above problem, Wu from Jin's group at the Changchun Institute of Optics, Fine Mechanics and Physics, proposed a grouping design method based on a combination of spatial ray tracing and aberration correction to construct an initial structure for an off-axis multi-reflective aspheric optical system [10]. This method uses the group design method for the optical system, the introduces aberration theory into the solution for each mirror group, corrects the third-order aberration of the optical system during the initial structure construction, and thus provides a starting point with optimization potential for the design of multi-mirror optical systems with extremely low aberration. However, because of the wide field of the lithographic projection optics, the optical system that is obtained by solving for the central field alone has a large aberration at the edge of the field. To solve this problem, the full-field aberration correction conditions can be added to the initial structure construction of the optical system.

In this paper, we propose a method to solve for the initial structure of an EUVL projection optics based on full-field aberration correction. First, the full field of the system is discretized, and a multi-objective evaluation function is established by combining the aberration theory with spatial ray tracing of the aberrations at the multi-characteristic field points and the structural constraints of the system. The initial structure of the EUVL projection optics is then solved for the established multi-objective evaluation function via the nondominated sorting and metaheuristics algorithm (NDSMA). After the initial structure produced by this approach was optimized, a final projection optical design with a numerical aperture (NA) of 0.33, full-field integrated wavefront error of 0.128 nm RMS, and full-field distortion of less than 1 nm was obtained, and the manufacturability of the system has been demonstrated through a tolerance analysis.

2. ESTABLISHMENT OF OBJECTIVE FUNCTION AND CALCULATION OF ABERRATION

A. Calculation of Aberration

To ensure that the initial structure obtained for the optical system satisfies both the full-field aberration correction condition and the spatial constraints, we use a combination of spatial ray tracing and aberration correction to establish an evaluation function for the field point aberration constraint and the system structure limit. The structure of a six-mirror optical system is shown in Fig. 1, and it consists of three main parts: the mask plane (object plane), the wafer plane (image plane), and six even-order aspherical mirrors that are coaxial and rotationally symmetric about the optical axis. The aperture pupil of the system is placed on mirror M_2 [11]. The ray emitted from the object plane at height y propagates via reflection from mirrors M_1, M_2, M_3, M_4, M_5, M_6 to reach the image plane at height y_{im}; the ratio of the image plane height to the object plane height should be equal to the ideal magnification β when the optical system is imaged ideally, and the optical system's ideal magnification $\beta = 0.25$ in this paper.

Assuming that the ratios of the apertures of the pairs of adjacent mirrors are $\alpha_1, \alpha_2, \alpha_3, \alpha_4, \alpha_5$, then the near-axis magnifications of the six mirrors can be expressed as $\beta_1, \beta_2, \beta_3, \beta_4, \beta_5, \beta_6$, and these parameters can be expressed using the following equations:

$$\begin{cases} \beta_1 = \frac{l_1'}{l_1} \approx \frac{u_1}{u_1'} \\ \beta_2 = \frac{l_2'}{l_2} \approx \frac{u_2}{u_2'} \\ \beta_3 = \frac{l_3'}{l_3} \approx \frac{u_3}{u_3'} \\ \beta_4 = \frac{l_4'}{l_4} \approx \frac{u_4}{u_4'} \\ \beta_5 = \frac{l_5'}{l_5} \approx \frac{u_5}{u_5'} \\ \beta_6 = \frac{l_6'}{l_6} \approx \frac{u_6}{u_6'} \end{cases} \quad \begin{cases} \alpha_1 = \frac{l_2}{l_1'} \approx \frac{h_2}{h_1} \\ \alpha_2 = \frac{l_3}{l_2'} \approx \frac{h_3}{h_2} \\ \alpha_3 = \frac{l_4}{l_3'} \approx \frac{h_4}{h_3} \\ \alpha_4 = \frac{l_5}{l_4'} \approx \frac{h_5}{h_4} \\ \beta_5 = \frac{l_6}{l_5'} \approx \frac{h_6}{h_5} \end{cases}, \tag{1}$$

where l_n, l_n', u_n, u_n' are the proximal axis object distance, the proximal axis image distance, the object-side aperture angle, and the image-side aperture angle of the first proximal axis ray when passing through the nth mirror, respectively; here h_n is the

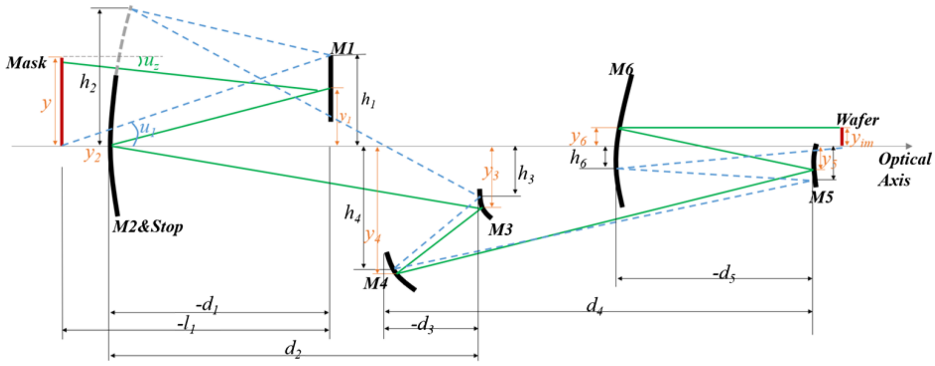

Fig. 1. Schematic diagram of the six-mirror optical system.

height of the intersection of the ray and the mirror when the first proximal axis ray that passes through the system reaches the nth mirror. According to the expressions above, the proximal axis object-image distance can be obtained for each mirror, and these distances can be expressed as follows:

$$\begin{cases} l_1' = \beta_1 l_1 \\ l_2' = \alpha_1\beta_1\beta_2 l_1 \\ l_3' = \alpha_1\alpha_2\beta_1\beta_2\beta_3 l_1 \\ l_4' = \alpha_1\alpha_2\alpha_3\beta_1\beta_3\beta_4 l_1 \\ l_5' = \alpha_1\alpha_2\alpha_3\alpha_4\beta_1\beta_2\beta_3\beta_4\beta_5 l_1 \\ l_6' = \alpha_1\alpha_2\alpha_3\alpha_4\alpha_5\beta_1\beta_2\beta_3\beta_4\beta_5\beta_6 l_1 \end{cases}$$

The relationship between the radius of curvature of each reflector and the system's structural parameters can easily be derived from the proximal axis equation, as follows:

$$r = \frac{(n'-n)l'l}{n'l - nl'}. \tag{3}$$

For a six-mirror optical system, the refractive index values of the light behind and in front of each surface can be expressed as $n_1 = n_3 = n_5 = n_2' = n_4' = n_6' = 1$, $n_2 = n_4 = n_6 = n_1' = n_3' = n_5' = -1$. When this expression is combined with Eq. (3), the radius of curvature can be calculated for each mirror, and the thicknesses d_1, d_2, d_3, d_4, d_5 of the optical system can be obtained from the paraxial optical theory as follows:

$$\begin{cases} r_1 = \frac{2\beta_1 l_1}{\beta_1+1} \\ r_2 = \frac{2\alpha_1\beta_1\beta_2 l_1}{\beta_2+1} \\ r_3 = \frac{2\alpha_1\alpha_2\beta_1\beta_2\beta_3 l_1}{\beta_3+1} \\ r_4 = \frac{2\alpha_1\alpha_2\alpha_3\beta_1\beta_2\beta_3\beta_4 l_1}{\beta_4+1} \\ r_5 = \frac{2\alpha_1\alpha_2\alpha_3\alpha_4\beta_1\beta_2\beta_3\beta_4\beta_5 l_1}{\beta_5+1} \\ r_6 = \frac{2\alpha_1\alpha_2\alpha_3\alpha_4\alpha_5\beta_1\beta_2\beta_3\beta_4\beta_5\beta_6 l_1}{\beta_6+1} \end{cases} \quad \begin{cases} d_1 = \beta_1 l_1 - \alpha_1\beta_1 l_1 \\ d_2 = \alpha_1\beta_1\beta_2 l_1 - \alpha_1\alpha_2\beta_1\beta_2 l_1 \\ d_3 = \alpha_1\alpha_2\beta_1\beta_2\beta_3 l_1 - \alpha_1\alpha_2\alpha_3\beta_1\beta_2\beta_3 l_1 \\ d_4 = \alpha_1\alpha_2\alpha_3\beta_1\beta_2\beta_3\beta_4 l_1 - \alpha_1\alpha_2\alpha_3\alpha_4\beta_1\beta_2\beta_3\beta_4 l_1 \\ d_5 = \alpha_1\alpha_2\alpha_3\alpha_4\beta_1\beta_2\beta_3\beta_4\beta_5 l_1 - \alpha_1\alpha_2\alpha_3\alpha_4\alpha_5\beta_1\beta_2\beta_3\beta_4\beta_5 l_1 \end{cases}. \tag{4}$$

In the case in which the above optical system structure parameters are known, the aberration theory can be used to calculate the third-order monochromatic aberrations of the system. The third-order aberrations mainly include spherical aberrations, coma, astigmatism, field curvature, and distortion, which are represented by S_I, S_{II}, S_{III}, S_{IV}, S_V and by the following expressions, respectively [12]:

$$\begin{cases} S_I = \sum hP + \sum h^4 K \\ S_{II} = \sum yP - J\sum W + \sum h^3 yK \\ S_{III} = \sum(y^2P/h) - 2J\sum(yW/h) + J^2\sum\phi + \sum h^2y^2K + J^2\sum(\Pi/h) \\ S_{IV} = J^2\sum(\Pi/h) \\ S_V = \sum(y^2P/h) - 3J\sum(y^2W/h^2) + J^2\sum(3y\phi + y\Pi/h)/h - J^3\sum(\Delta(1/n^2))/h^2 + \sum hy^3K \end{cases},$$

$$P = \left(\frac{\Delta u}{\Delta\frac{1}{n}}\right)^2 \Delta\frac{u}{n} \quad W = \left(\frac{\Delta u}{\Delta\frac{1}{n}}\right)\Delta\frac{u}{n},$$

$$\Pi = \frac{\Delta(nu)}{nn'}, \quad \phi = \frac{1}{h}\Delta\frac{u}{n}, \quad K = \frac{k}{r^3}\Delta n, \quad J = nuy, \tag{5}$$

where y_1, y_2, y_3, y_4, y_5, y_6 are the heights of the intersection points of the second proximal rays with each of the mirrors M_1, M_2, M_3, M_4, M_5, M_6, respectively, as they propagate through the system, and k represents the conics of each mirror. By combining Eq. (4) with the aberration equation above,

$$\begin{cases} l_1 = l_1 \\ l_2 = \alpha_1\beta_1 l_1 \\ l_3 = \alpha_1\alpha_2\beta_1\beta_2 l_1 \\ l_4 = \alpha_1\alpha_2\alpha_3\beta_1\beta_2\beta_3 l_1 \\ l_5 = \alpha_1\alpha_2\alpha_3\alpha_4\beta_1\beta_2\beta_3\beta_4 l_1 \\ l_6 = \alpha_1\alpha_2\alpha_3\alpha_4\alpha_5\beta_1\beta_2\beta_3\beta_4\beta_5 l_1 \end{cases}. \tag{2}$$

we can find symbolic solutions for the five different third-order aberrations of the six-reflector optical system; refer to Appendix A for full details. Next, the aberration correction evaluation function of the optical system can be established, and this function is expressed as $\text{Const}_{\text{Aberration}} = |S_I| + |S_{II}| + |S_{III}| + |S_{IV}| + |S_V|$.

B. Establishment of the Multi-Featured Field Point Evaluation Function

As shown in Fig. 2, the EUVL projection optics uses a highly off-axis annular FOV, where the height of the central field is 140 mm and the area of the full field is 8 mm × 104 mm, which makes the system much more tolerant of field curvature, astigmatism, and aberrations [13].

To characterize the full-field imaging performance accurately while also considering the complexity of the calculations, nine characteristic field points were selected from within the full-field range. As shown in Fig. 3, the central field coordinates of the system are (0,140), and the remaining characteristic field coordinates are listed in Table 1. Because the annular FOV is

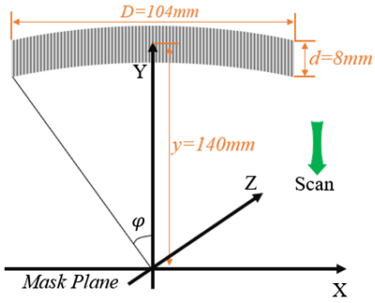

Fig. 2. Schematic diagram of the full field of the EUVL objective.

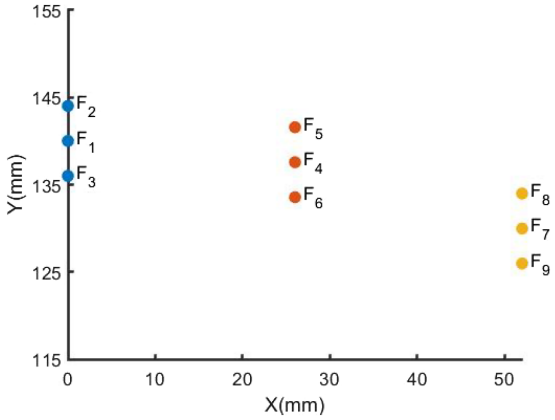

Fig. 3. Sampling schematic of the nine characteristic field points.

symmetrical about the meridian plane, the characteristic field point is chosen to be unilateral with respect to the full field, which contains both the contour of the half-field and the central annular band.

The evaluation function for a single field point consists of two parts. The first part is the third-order aberration value obtained using the aberration theory and, when the five third-order aberration values of the system converge toward zero during the optimization process, the system has completed correction of the aberration. The second part is the system structure constraint obtained using spatial ray tracing, which includes the limit of the unobstructed light, the stop position constraint, the image plane position constraint, and the object distance constraint; additionally, to ensure that the overlay is minimized when the wafer is defocused, it is necessary to ensure image telecentricity. The evaluation function for a single field point can be expressed using the form of Eq. (6):

$$\text{Fitness} = \text{Const}_{\text{Aberration}} + \text{Const}_{\text{Structure}}, \tag{6}$$

where $\text{Const}_{\text{Aberration}}$ is the third-order aberration constraint, and $\text{Const}_{\text{Syructure}}$ is the system structure constraint.

Using the method introduced above to determine the evaluation functions, constrained evaluation functions are established for the characteristic field points, and these evaluation functions can be divided into two categories: the central field (F1) evaluation function and other field (F2–F9) evaluation functions.

1. Central field objective function: the central field plays a major role in the design of optical systems. We use the weighted sum of the constraints of the third-order aberration $\text{Const}_{\text{Aberration}}$, the stop position $\text{Const}_{\text{stop}}$, the image telecentricity of the center field Te_{F_1}, the thicknesses of each of the mirrors $\text{Const}_{\text{dis}}$, and the magnification Const_{β} as the prime constraint function; this determines the basic structure of the entire optical system during the optimal solution process, while also ensuring that the third-order aberration of the center field, which is the most important aberration in the system, can be corrected. Its fitness function can then be expressed as follows:

$$\begin{aligned}\text{Fitness}_1 = {} & W_{1,1}\text{Const}_{\text{Aberration},F_1} + W_{1,2}\text{Const}_{\text{Stop}} \\ & + W_{1,3}\text{Const}_{Te,F_1} + W_{1,4}\text{Const}_{\text{dis}} \\ & + W_{1,5}\text{Const}_{\beta} + W_{1,6}\text{Const}_{\text{other}},\end{aligned} \tag{7}$$

where $W_{1,n}$ represents the weight values corresponding to the different constraints in the evaluation function for the central field, and the weights of different constraints can be adjusted to control the degree to which the system satisfies these constraints; $\text{Const}_{\text{other}}$ indicates the values of other constraints.

2. Other fields objective function: the other field points mainly control the third-order aberration under the full field, while the telecentricity of each field point on the image plane is another of the elements to be controlled. To ensure that the rays passing through the optical system are not occluded by the edges of its surfaces, we introduce the concept of spatial ray tracing. By tracing the rays emitted from various characteristic fields and using the height at which they reach each mirror surface as a constraint, the height at which the rays reach a certain surface is constrained to be outside the effective aperture of that surface. This constraint is denoted as $\text{Const}_{\text{OBS}}$. The following equation gives an expression for the fitness function of the edge field points:

$$\begin{aligned}\text{Fitness}_i = {} & W_{i,1}\text{Const}_{\text{Aberration},F_i} + W_{i,2}\text{Const}_{Te,F_i} \\ & + W_{i,3}\text{Const}_{\text{obs}},\end{aligned} \tag{8}$$

where i is the number of fields.

The expressions for the evaluation function above show that the multi-field third-order aberration of the initial structure of the optical system is corrected, and that the structural constraints of the system are fulfilled when the system satisfies the

Table 1. Coordinate Values of Nine Characteristic Field Points

Field	X/mm	Y/mm
F1	0	140
F2	0	144
F3	0	136
F4	26	137.56
F5	26	141.56
F6	26	133.56
F7	52	129.98
F8	52	133.98
F9	52	125.98

equations, i.e., when $\text{Fitness}_i = 0 (i = 1 \sim 9)$. However, the ideal presented result above is difficult to achieve during the actual design process. If some algorithm is available that can cause the characteristics of the field of the fitness function above to be as close as possible to a minimum value, then the aberration correction will be better, and the system structure will also meet the design requirements. Therefore, solving the multi-field point optical evaluation function to ensure that the third-order aberration value of the optical system converges to zero is the key to the realization of full-field aberration correction.

3. SOLVING THE FITNESS FUNCTION FOR MULTIPLE FIELDS VIA NDSMA

The nondominated sorting method was first proposed by Srinivas and Deb in 1995 [14], was subsequently improved by Agrawal *et al*. in 2000, and was then applied as described in the literature [15]. Nondominated sorting provides a faster and more rational ranking principle for evolution and selection of elite individuals within a population during multi-objective optimization. This method can then extend the application of traditional single-objective optimization algorithms such as the least squares algorithm, genetic algorithms, and the particle swarm algorithm to the solution of multi-objective functions, and it is more applicable to realistic multi-objective optimization problems with high complexity. Metaheuristic algorithms (MAs) are a class of algorithms that mimic natural behavior and phenomena [16]. MAs can find optimal/near-optimal solutions because of advantages that include ease of implementation, flexibility, avoidance of traps in local optima, and suitability for use as a black box, but they cannot be applied to the problem of multi-objective evaluation function optimization. Combining the advantages of the ease of implementation of an MA and its high solution space optimization capability with the excellent sorting and screening abilities of the nondominated sorting method for elite individuals in a population, we propose the use of the NDSMA for the solution of the aberration correction problem for multiple characteristic field points. This breaks the limitation of the traditional optical system initial structure solution methods that can only control a single-objective function.

In this paper, the NDSMA is used to solve for the constraints of the multiple characteristic field points of the EUVL projection optics, and this algorithm includes 21 system variables, which are $\alpha_1, \alpha_2, \alpha_3, \alpha_4, \alpha_5$, and $\beta_1, \beta_2, \beta_3, \beta_4, \beta_5, \beta_6, k_1, k_2, k_3, k_4, k_5, k_6, l_1, y, u_z, u_1$. The specific code for this algorithm can be found in Appendix B, and the detailed code for nondominated sorting of the nine fitness function values of the individuals in NDSMA can be found in Appendix C. The flow chart for the solution for the NDSMA is shown in Fig. 4, and the specific steps are described as follows:

Step 1: initialize the initial parameters of the algorithm and the positions of the individuals. The algorithm contains three initial parameters, C_1, C_2, C_3, which determine the convergence and the degree of variation in the position coordinates of the individuals when the population is iterated under different behavioral conditions. At the same time, the initialized population must be established, and the coordinates of the individuals in the population are selected at random from within the set variables.

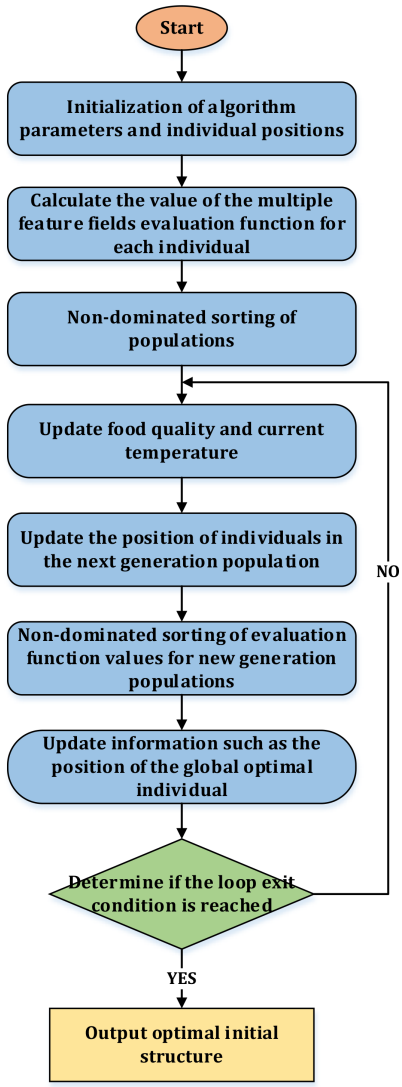

Fig. 4. Flow chart for the NDSMA.

Step 2: calculate the value of the multi-objective evaluation function that corresponds to each individual. The evaluation function value calculation framework is constructed based on the method used to establish the evaluation function for multiple characteristic field points in the previous section; the multi-objective evaluation function value for each individual is then calculated using this framework.

Step 3: perform nondominated sorting of all individuals in the population. All individuals in the population are assigned dominance levels according to their individual rankings, as given in Appendix C, where higher dominance levels imply that the individuals better satisfy the multi-objective constraints; the position information for the optimal individuals in the population and the fitness information of the characteristic field must also be recorded.

Step 4: update the food quality and the current temperature. Different food quality and environmental temperature values are generated during each population iteration, and these values determine which of the individuals in the population are to

perform the different activities. The food quality Q and the environmental temperature Temp can be obtained using the following equations:

$$\text{Temp} = e^{-\frac{\text{Iter}}{N_I}}, \quad Q = C_1 e^{\frac{\text{Iter}-N_I}{N_I}}, \tag{9}$$

where Iter is the current number of iterations, and N_I denotes the maximum number of iterations.

Step 5: update the positions of the individuals in the next generation of the population. The environmental temperature Temp and the food quality Q that were calculated in Step 4 determine the way in which the parent population generates the next generation of the population when the solution framework reaches a specific threshold, and the detailed method for updating the location of the next generation of the population can be found in Appendix B.

Step 6: calculate the fitness values of the individuals in the new generation of the population; they must then be ranked via nondominated sorting, and information about the individuals with the best dominance levels in the new generation of the population must be recorded.

Step 7: update the global optimal individual position information. Compare the evaluation function value of the best individual in the new generation of the population with the current global best individual, where the evaluation function value corresponding to the central field point is the high weight evaluation index, and the evaluation function value that corresponds to the edge field is the auxiliary evaluation index; then rank the combined evaluation function value of the two individuals above. If the value of the composite evaluation function of the best individual in the new generation of the population is better than that of the current global best individual, then the global best individual is replaced with the best individual from the new generation of the population.

Step 8: determine if the end condition of the iteration has been reached. If the loop iteration reaches the exit condition, which is generally the predefined maximum number of iterations, then the loop is exited, and the best initial system structure is output; otherwise, if the exit condition is not reached, the loop then executes Step 4 to Step 8 until the end-of-iteration condition is met.

4. DESIGN RESULTS AND TOLERANCE ANALYSIS

A. Design Results

The multi-objective function is established based on the third-order monochromatic aberration values for the nine characteristic field points that can represent the full-field image quality and the structural constraints of the optical system, and the initial structure of the EUVL projection optics is then resolved using the NDSMA, as described in Section 3. The initial parameters for the algorithm are $C_1 = 1.8$, $C_2 = 2$, and $C_3 = 0.6$, the maximum number of iterations is 50, and the population size was set at 500. The time consumed by the execution of the algorithm was 6 min.

Figure 5 shows the convergence curve of the fitness function, where the *Fitness of Chief Field* is the value of the central field evaluation function that corresponds to the global best individual in the current population, and the *Fitness of Edge Field* represents the average of the remaining field evaluation function values. The evolution of the curve shows that the algorithm has reached the final convergence value at the 15th iteration and that the evaluation function values of all feature fields of the system converge to a minimal value, indicating that the algorithm converges rapidly. The values of the algorithm parameters that correspond to the initial structure of EUVL projection optics obtained using the algorithm are shown in Table 2, and the structure is shown in Fig. 6.

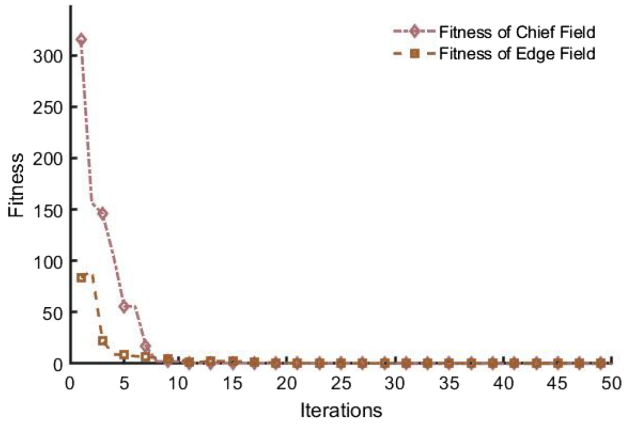

Fig. 5. Fitness function convergence curve.

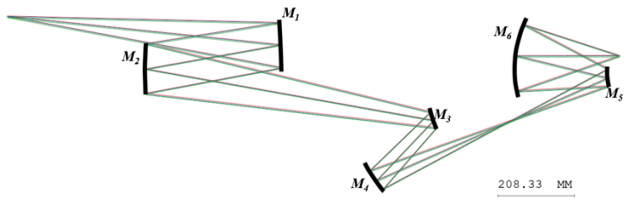

Fig. 6. Schematic diagram of the initial system structure.

Table 2. Variable Values of the Algorithm

Parameter	Value	Parameter	Value	Parameter	Value
α_1	1.090	β_3	1.064	k_4	0.049
α_2	0.360	β_4	0.630	k_5	6.975
α_3	1.504	β_5	−0.303	k_6	0.076
α_4	−0.679	β_6	0.941	l_1	750
α_5	3.828	k_1	−0.440	u_1	−0.083
β_1	−5.526	k_2	1.851	u_z	0.101
β_2	0.265	k_3	−0.089	y	140

The five third-order aberration values for the nine characteristic field points of the system are obtained using the aberration theory, with results as shown in Fig. 7, where parts (a)–(e) represent the distributions of third-order monochromatic aberrations $S_I \sim S_V$, respectively, and part (f) represents the overall distribution of the aberrations in the system. The figure illustrates that the third-order aberration is corrected well over the full field and that the values of the aberrations are close to zero.

Further optimization of the EUVL system was then performed based on the initial structure obtained above. During the optimization process, the chief ray distortion and the

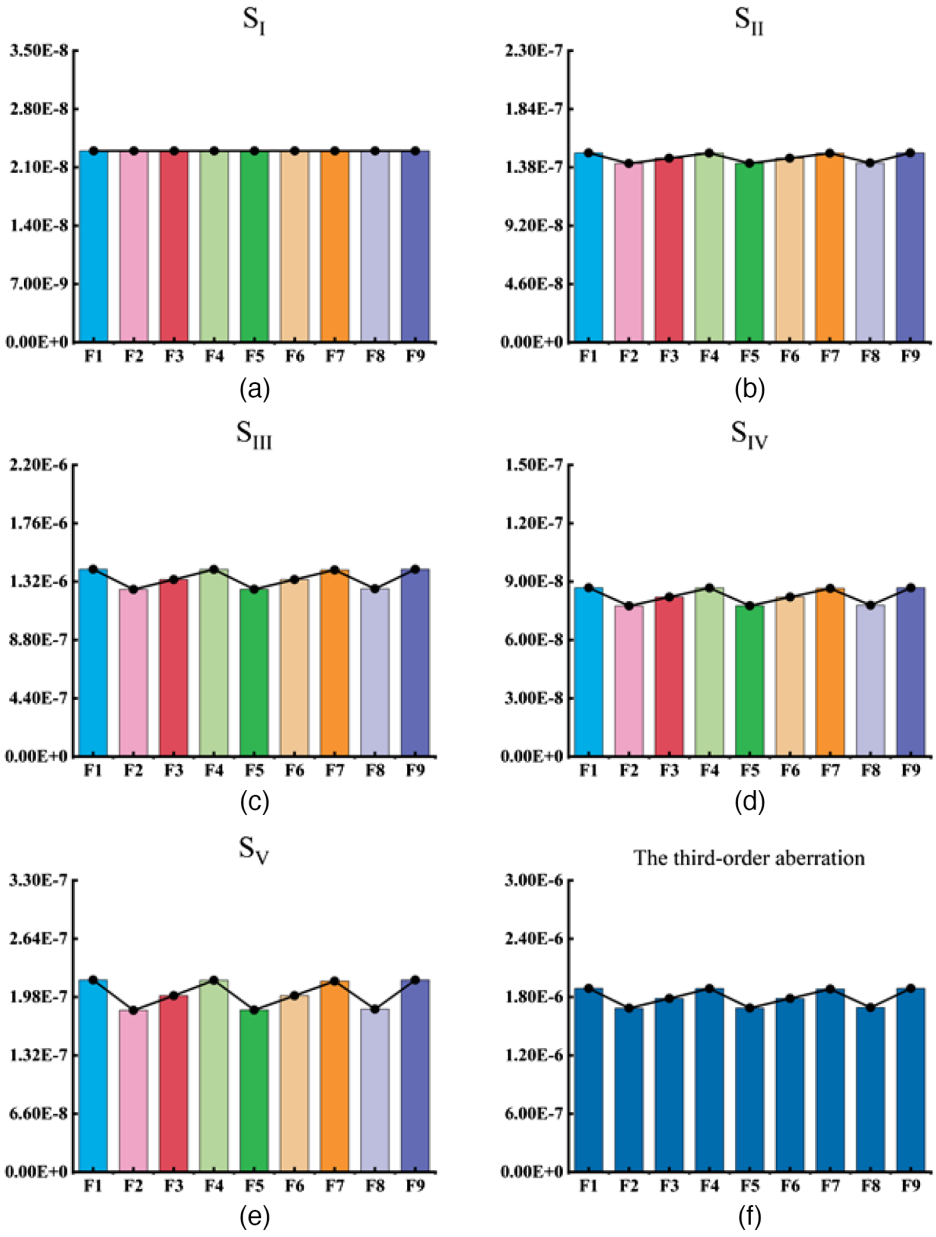

Fig. 7. Aberration distributions for the characteristic field points.

telecentricity of the system are limited, and the back working distance of the objective is controlled while satisfying the requirement for an unobstructed beam.

To evaluate the system's full-field imaging quality more accurately and more comprehensively, it is necessary to perform more intensive sampling over the full field. The object field shown in Fig. 2 was sampled uniformly, as shown in Fig. 8, and the full field was divided into 13 equal parts in the x direction and five equal parts in the y direction.

A schematic diagram of the optimized structure of the extremely low aberration full-field EUVL projection optics is shown in Fig. 9. An analysis of the wavefront aberrations and distortions obtained from 65 sampled FOVs indicates that the RMS wavefront error value of the optimized EUVL projection optics is 0.128 nm, and the maximum distortion is 1 nm. The distributions of the chief ray distortion and the wavefront

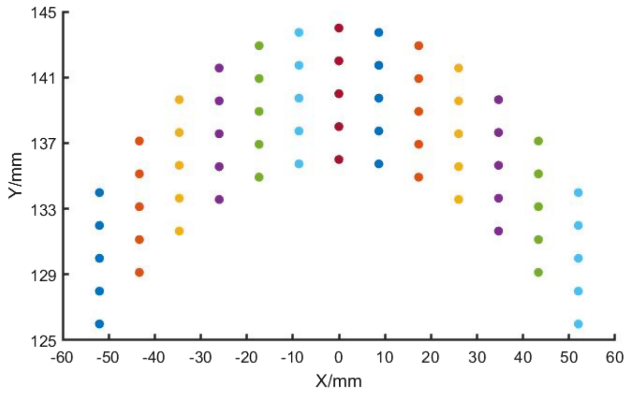

Fig. 8. Schematic diagram of 5 × 13 field points.

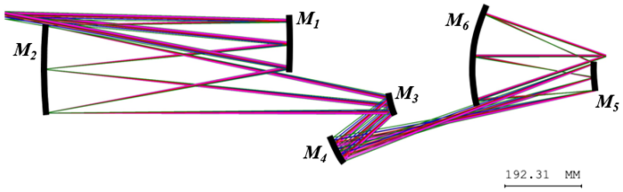

Fig. 9. Schematic diagram of the optimized structure for the EUVL system.

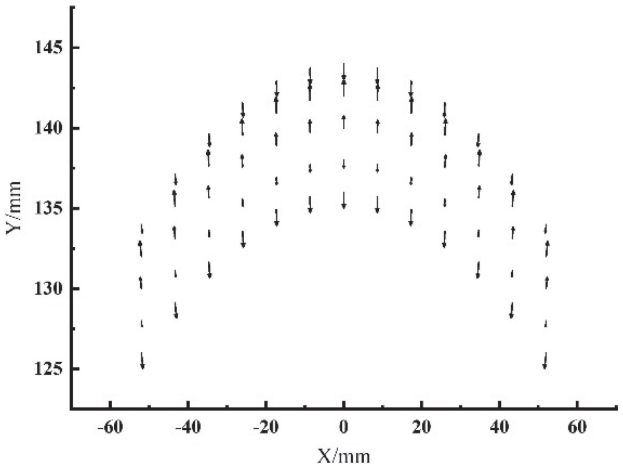

Fig. 10. Distortion distribution of the full field.

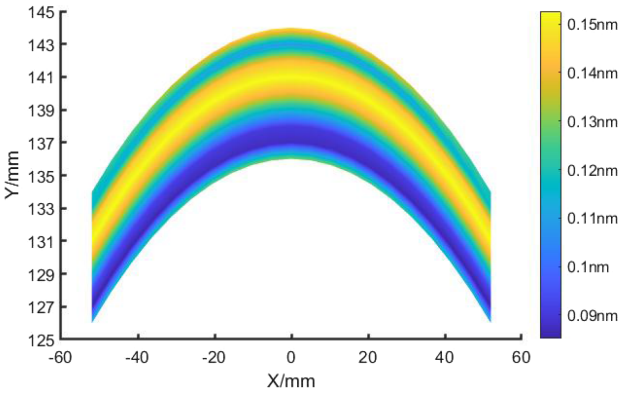

Fig. 11. RMS wavefront error on the full field.

error are shown in Figs. 10 and 11, respectively. The imaging performance parameters of the system are listed in detail in Table 3.

B. Tolerance Analysis

As an ultra-high-precision optical system, the EUVL projection optics has extremely strict requirements for assembly tolerance. The precision of component spacing and tilt detection accuracy must reach the level of micrometers and milliradians. In order to ensure that the projection lens system can meet the high imaging quality requirements, strict control of processing and assembly tolerances is necessary, and suitable compensating components need to be selected to compensate for the degradation of imaging quality caused by assembly errors, while relaxing the strict requirements for tolerances.

Table 3. Specifications of the Optimized EUVL Projection Optics Structure

Parameter	Specifications
Wavelength	13.5 nm
Object-side FOV	8 mm × 104 mm
Magnification	0.25
Numerical aperture	0.33
MIN_{OBS}[a]	5 mm
Wavefront error RMS	0.128 nm
Max distortion	1 nm
Max telecentricity error	1.987 mrad
Back working distance	30 mm
Total track	1500 mm

[a]Minimum distance between the marginal ray and the boundary for each mirror.

Table 4. Tolerance Range of the System

Mirror	DLZ/μm	DLX/μm	DLY/μm	DLA/μrad	DLB/μrad
M1	±1	±1	±±1	±2	±2
M2	±1	±1	±1	±2	±2
M3	—	—	—	±5	±5
M4			Alignment datum		
M5	±0.5	±1	±1	±2	±2
M6	±0.5	—	—	±1	±1

A tolerance analysis is performed on the lens system based on the nine characteristic fields introduced in Section 2.B. Before performing the tolerance analysis, an inverse sensitivity analysis of the system is conducted to determine M3 and M6 as compensating elements. As M4 has an effective aperture far from the optical axis and is sensitive to aberrations, it was used as the alignment reference surface for the EUVL projection lens system. Using the criterion of full-field wavefront RMS value less than 0.035λ, the system was analyzed for tolerance within the ranges shown in Table 4, utilizing the Wavefront Differential Tolerance Analysis feature in the Code V optical design software.

The (DLZ), (DLX), and (DLY) in the table, respectively, represent the eccentricity of the component along the z axis, x axis, and y axis of the local coordinates on the surface. DLA and DLB represent the tilt of the component around the z axis and y axis of the local coordinates. "—" is used as a compensator for this item.

Figure 12 shows the cumulative probability distribution curve of the full-field wavefront RMS of the EUVL projection optics. Within the designed tolerance range, the assembled system has a 90% probability of meeting the requirement of full-field wavefront error RMS $< 0.031\lambda$, and a 95% probability of full-field wavefront error RMS $< 0.035\lambda$, which satisfies the lithography requirements. The above results indicate that even though the EUV lithography projection system has extremely strict requirements for assembly, the EUVL system constructed using the optical system construction method proposed in this paper has good manufacturability under the current level of processing and assembly.

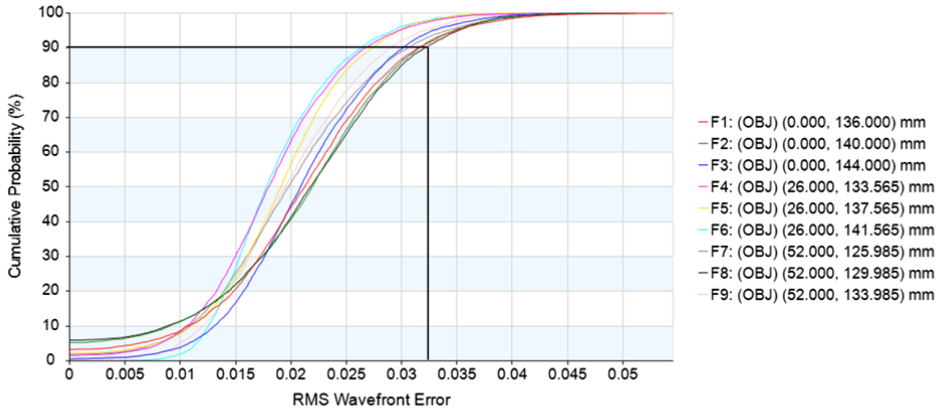

Fig. 12. Cumulative probability distribution curve of the wavefront error.

5. CONCLUSION

With the aim of satisfying the strict full-field aberration requirements for an EUVL projection optics, we have proposed a method to construct the initial structure of a reflective optical system based on full-field aberration correction. This method combines the aberration theory with spatial ray tracing to correct the aberrations of multi-characteristic field points, which can represent the aberration distribution for the full FOV and establishes an evaluation function for aberration control and system constraints. The NDSMA is used to solve the multi-objective optimization problem in this paper. Then a reasonable initial structure for the six-mirror system with a corrected third-order aberration in the full field is obtained. The optimized structure has a full-field RMS wavefront error of 0.128 nm, and its chief ray distortion is less than 1 nm after a further tolerance analysis, the data indicate that the system is manufacturable at current levels of machining and assembly, which verifies the effectiveness of the method for construction of the initial optical system structure based on the full-field aberration correction proposed in this paper. The solution method that we propose here also provides theoretical ideals for a solution of other initial structure problems involving optical systems with multi-objective constraint requirements.

APPENDIX A: SYMBOLIC SOLUTIONS FOR THE THIRD-ORDER ABERRATION

$$
\begin{aligned}
S_I = {} & \frac{(1+\beta_1)\beta_2\beta_3\beta_4\beta_5(1+2\beta_1(-1+k_1)+k_1+\beta_2^2(1+k_1))l_1u_1^3}{8\beta_1^2} - \frac{1}{8\beta_1^2\beta_2^2\beta_3^2\beta_4^2\beta_5^2\beta_6^2}\alpha_1\big((1+\beta_1)\beta_2^3\beta_3^3\beta_4^3\beta_5^3 \\
& \times \big(1+2\beta_2(-1+k_2)+k_2+\beta_2^2(1+k_2)\big) + \alpha_2\big(-(1+\beta_3)\beta_4^3\beta_5^3\beta_6^3\big(1+2\beta_3(-1+k_3)+k_3+\beta_3^2(1+k_3)\big) + \alpha_3\big((1+\beta_4) \\
& \times \beta_5^3\beta_6^3\big(1+2\beta_4(-1+k_4)+k_4+\beta_4^2(1+k_4)\big) + \alpha_4\big(-(1+\beta_5)\beta_6^3\big(1+2\beta_5(-1+k_5)+k_5+\beta_5^2(1+k_5)\big) + \alpha_5(1+\beta_6)\big) \\
& \times \big(1+2\beta_6(-1+k_6)+k_6+\beta_6^2(1+k_6)\big)\big)\big)\big)l_1u_1^3
\end{aligned}
$$

$$
\begin{aligned}
S_{II} = {} & -\frac{1}{8\beta_1^2\beta_2^2\beta_3^2\beta_4^2\beta_5^2\beta_6^2}3u_1^2\big(\beta_1^2\beta_2^3\beta_3^3\beta_4^3\beta_5^3\beta_6^3(1-3k_1)y_1 + \beta_1(-2\beta_2\beta_3\beta_4\beta_5\beta_6 y + \beta_2^3\beta_3^3\beta_4^3\beta_5^3\beta_6^3(1-3k_1)y_1) \\
& + \beta_1^3\beta_2^3\beta_3^3\beta_4^3\beta_5^3\beta_6^3(2y-(1+k_1)y_1) + \beta_3^3\beta_4^3\beta_5^3\beta_6^3 y_2 + \beta_3^3\beta_4^3\beta_5^3\beta_6^3 k_2 y_2 + \beta_2\beta_3^3\beta_4^3\beta_5^3(-1+3k_2)y_2 + \beta_2^2\beta_3^3 \\
& \times \beta_4^3\beta_5^3\beta_6^3(-1+3k_2)y_2 + \beta_2^3\beta_3^3\beta_4^3\beta_5^3\beta_6^3(-(1+k_1)y_1+(1+k_2)y_2) - \beta_4^3\beta_5^3\beta_6^3 y_3 + \beta_4^3\beta_5^3\beta_6^3 y_3 + \beta_3\beta_4^3\beta_5^3\beta_6^3 \\
& \times y_3 - \beta_3^2\beta_4^3\beta_5^3\beta_6^3 y_3 - \beta_4^3\beta_5^3\beta_6^3 k_3 y_3 - 3\beta_3\beta_4^3\beta_5^3\beta_6^3 k_3 y_3 - 3\beta_4^3\beta_5^3\beta_6^3 k_3 y_3 - \beta_4^3\beta_5^3\beta_6^3 k_3 y_3 + \beta_5^3\beta_6^3 y_4 - \beta_4\beta_5^3 \\
& \times \beta_6^3 y_4 - \beta_4^2\beta_5^3\beta_6^3 y_4 + \beta_4^3\beta_5^3\beta_6^3 y_4 + \beta_5^3\beta_6^3 k_4 y_4 + 3\beta_4\beta_5^3\beta_6^3 k_4 y_4 + 3\beta_4^2\beta_5^3\beta_6^3 k_4 y_4 + \beta_4^3\beta_5^3\beta_6^3 k_4 y_4 - \beta_6^3 y_5 \\
& + \beta_5\beta_6^3 y_5 + \beta_5^2\beta_6^3 y_5 - \beta_5^3\beta_6^3 y_5 - \beta_6^3 k_5 y_5 - 3\beta_5\beta_6^3 k_5 y_5 - 3\beta_5^2\beta_6^3 k_5 y_5 - \beta_5^3\beta_6^3 k_5 y_5 + y_6 - \beta_6 y_6 - \beta_6^2 y_6 + \beta_6^3 y_6 \\
& + k_6 y_6 + 3\beta_6 k_6 y_6 + \beta_6^2 k_6 y_6\big)
\end{aligned}
$$

$$S_{III}=\frac{1}{(8\alpha_1\alpha_2\alpha_3\alpha_4\alpha_5\beta_1^2\beta_2^2\beta_3^2\beta_4^2\beta_5^2\beta_6^2 l_1)}\big(u_1(-\alpha_1\alpha_2\alpha_3\alpha_4\alpha_5\beta_2^3\beta_3^3\beta_4^3\beta_5^3\beta_6^3 y_1\big(-4\beta_1(-1+\beta_1^2)y+(1+\beta_1)$$
$$\times\big((-1+\beta_1)^2+(1+\beta_1)^2k_1\big)y_1\big)+\alpha_2\alpha_3\alpha_4\alpha_5(1+\beta_2)\beta_3^3\beta_4^3\beta_5^3\beta_6^3 y_2\big(4\beta_1(-1+\beta_2)\beta_2 y+\big((-1+\beta_2)^2+(1+\beta_2)^2k_2\big)y_2\big)$$
$$-4\alpha_3\alpha_4\alpha_5\beta_1\beta_2\beta_3\beta_4^3\beta_5^3\beta_6^3 yy_3+4\alpha_3\alpha_4\alpha_5\beta_1\beta_2\beta_3^3\beta_4^3\beta_5^3\beta_6^3 yy_3-\alpha_3\alpha_4\alpha_5\beta_4^3\beta_5^3\beta_6^3 y_3^2+\alpha_3\alpha_4\alpha_5\beta_3\beta_4^3\beta_5^3\beta_6^3 y_3^2$$
$$+\alpha_3\alpha_4\alpha_5\beta_3^2\beta_4^3\beta_5^3\beta_6 y_3^2-\alpha_4\alpha_5\beta_3^3\beta_4^3\beta_5^3\beta_6^3 y_3^2-\alpha_4\alpha_5\beta_4^3\beta_5^3\beta_6^3 k_3 y_3^2-3\alpha_3\alpha_4\alpha_5\beta_3\beta_4^3\beta_5^3\beta_6^3 k_3 y_3^2-3\alpha_3\alpha_4\alpha_5\beta_3^2\beta_4^3$$
$$\times\beta_5^3\beta_6^3 k_3 y_3^2-\alpha_3\alpha_4\alpha_5\beta_3^3\beta_4^3\beta_5^3\beta_6^3 k_3 y_3^2-4\alpha_4\alpha_5\beta_1\beta_2\beta_3^3\beta_5^3\beta_6^3 yy_4+\alpha_4\alpha_5\beta_1\beta_2\beta_3\beta_4^3\beta_5^3\beta_6^3 yy_4+\alpha_4\alpha_5\beta_5^3\beta_6^3 y_4^2$$
$$-\alpha_4\alpha_5\beta_4\beta_5^3\beta_6^3 y_4^2-\alpha_4\alpha_5\beta_4^2\beta_5^3\beta_6^3 y_4^2+\alpha_4\alpha_5\beta_4^3\beta_5^3\beta_6^3 y_4^2+3\alpha_4\alpha_5\beta_5^3\beta_6^3 k_4 y_4^2+3\alpha_4\alpha_5\beta_5^3\beta_6^3 k_4 y_4^2+\alpha_4\alpha_5\beta_4^3\beta_5^3$$
$$\times\beta_6 c^3 k_4 y_4^2-4\alpha_5\beta_1\beta_2\beta_3\beta_4\beta_5\beta_6^3 yy_5+4\alpha_5\beta_1\beta_2\beta_3\beta_4\beta_5^3\beta_6^3 yy_5-\alpha_5\beta_6^3 y_5^2+\alpha_5\beta_5\beta_6^3 y_5^2+\alpha_5\beta_5^2\beta_6^3 y_5^2-\alpha_5\beta_5^3\beta_6^3 y_5^2$$
$$-\alpha_5\beta_6^3 k_5 y_5^2-3\alpha_5\beta_5\beta_6^3 k_5 y_5^2-3\alpha_5\beta_5^2\beta_6^3 k_5 y_5^2-\alpha_5\beta_5^3\beta_6^3 k_5 y_5^2+4\beta_1\beta_2\beta_3\beta_4\beta_5\beta_6(-1+\beta_6^2)yy_6+(1+\beta_6)$$
$$\times\big((-1+\beta_6)^2+(1+\beta_6)^2k_6\big)y_6^2\big)\big)$$

$$S_{IV}=\frac{1}{2\alpha_1\alpha_2\alpha_3\alpha_4\alpha_5 l_1}(-1+(-1+\alpha_5(1+\beta_5+\alpha_4(-1+(-1+\alpha_3(1+\beta_3$$
$$+\alpha_2(-1+(-1+\alpha_1+\alpha_1\beta_1)\beta_2)\beta_3))\beta_4)\beta_5))\beta_6)u_1y^2$$

$$S_V=\frac{1}{(8\alpha_1^2\alpha_2^2\alpha_3^2\alpha_4^2\alpha_5^2\beta_1^2\beta_2^2\beta_3^2\beta_4^2\beta_5^2\beta_6^2 {l_1}^2)}\big(\alpha_1^2\alpha_2^2\alpha_3^2\alpha_4^2\alpha_5^2(1+\beta_1)\beta_2^3\beta_3^3\beta_4^3\beta_5^3\beta_6^3 y_1\big((1+k_1)y_1^2$$
$$+2\beta_1 y_1(3y+(-1+k_1)y_1)+\beta_1^2(8y^2-6yy_1+(1+k_1)y_1^2)\big)-\alpha_2^2\alpha_3^2\alpha_4^2\alpha_5^2(1+\beta_1)\beta_2^3\beta_3^3\beta_4^3\beta_5^3 y_2\big(8\beta_1^2\beta_2^2y^2$$
$$+6\beta_1(-1+\beta_2)\beta_2 yy_2+\big(1+2\beta_2(-1+k_2)+k_2+\beta_2^2(1+k_2)\big)y_2^2\big)+8\alpha_3^2\alpha_4^2\alpha_5^2\beta_1^2\beta_2^2\beta_3^2\beta_4^3\beta_5^3\beta_6^3 y^2y_3+8\alpha_3^2\alpha_4^2$$
$$\times\alpha_5^2\beta_1^2\beta_2^2\beta_3^3\beta_4^3\beta_5^3\beta_6^3 y^2y_3+6\alpha_3^2\alpha_4^2\alpha_5^2\beta_1\beta_2\beta_3\beta_4^3\beta_5^3\beta_6^3 yy_3^2-6\alpha_3^2\alpha_4^2\alpha_5^2\beta_1\beta_2\beta_3^3\beta_4^3\beta_5^3\beta_6^3 yy_3^2+\alpha_3^2\alpha_4^2\alpha_5^2$$
$$\times\beta_4^3\beta_5^3\beta_6^3 y_3^3-\alpha_3^2\alpha_4^2\alpha_5^2\beta_3\beta_4^3\beta_5^3\beta_6^3 y_3^3-\alpha_3^2\alpha_4^2\alpha_5^2\beta_3^2\beta_4^3\beta_5^3\beta_6^3 y_3^3+\alpha_3^2\alpha_4^2\alpha_5^2\beta_3^3\beta_4^3\beta_5^3\beta_6^3 y_3^3+\alpha_5^2\beta_4^3\beta_5^3$$
$$\times\beta_6^3 k_3 y_3^3+3\alpha_3^2\alpha_4^2\alpha_5^2\beta_3\beta_4^3\beta_5^3\beta_6^3 k_3 y_3^3+3\alpha_3^2\alpha_4^2\alpha_5^2\beta_3^2\beta_4^3\beta_5^3\beta_6^3 k_3 y_3^3+\alpha_3^2\alpha_4^2\alpha_5^2\beta_3^3\beta_4^3\beta_5^3\beta_6^3 k_3 y_3^3-8\alpha_4^2\alpha_5^2$$
$$\times\beta_2^2\beta_3^2\beta_4^2\beta_5^3\beta_6^3 y^2y_4-8\alpha_4^2\alpha_5\beta_3^2\beta_4^3\beta_5^3\beta_6^3 y^2y_4+6\alpha_5^2\beta_1\beta_2\beta_3\beta_4\beta_5^3\beta_6^3 yy_4^2-6\alpha_5^2\beta_1\beta_2\beta_3\beta_4^3\beta_5^3\beta_6^3 yy_4^2-\alpha_5^2\beta_5^3$$
$$\times\beta_6^3 y_4^3+\alpha_4^2\alpha_5^2\beta_4\beta_5^3\beta_6^3 y_4^3+\alpha_4^2\alpha_5^2\beta_4^2\beta_5^3\beta_6^3 y_4^3+\alpha_4^2\alpha_5^2\beta_4^3\beta_5^3\beta_6^3 y_4^3-\alpha_4^2\alpha_5^2\beta_5^3\beta_6^3 k_4 y_4^3-3\alpha_4^2\alpha_5^2\beta_4\beta_5^3\beta_6^3$$
$$\times k_4 y_4^3-3\alpha_4^2\alpha_5^2\beta_4^2\beta_5^3\beta_6^3 k_4 y_4^3-\alpha_4^2\alpha_5^2\beta_4^3\beta_5^3\beta_6^3 k_4 y_4^3+8\alpha_5^2\beta_1^2\beta_2^2\beta_3^2\beta_4^2\beta_5^2\beta_6^3 y^2y_5+8\alpha_5^2\beta_1^2\beta_2^2\beta_3^2\beta_4^2\beta_5^3\beta_6^3$$
$$\times y^2y_5+6\alpha_5^2\beta_1\beta_2\beta_3\beta_4\beta_5\beta_6^3 yy_5^2-6\alpha_5^2\beta_1\beta_2\beta_3\beta_4\beta_5^3\beta_6^3 yy_5^2+\alpha_5^2\beta_6^3 y_5^3-\alpha_5^2\beta_5\beta_6^3 y_5^3+\alpha_5^2\beta_5^3\beta_6^3 y_5^3+\alpha_5^2\beta_5^3 k_5 y_5^3$$
$$+3\alpha_5^2\beta_5\beta_6^3 k_5 y_5^3+3\alpha_5^2\beta_5^2\beta_6^3 k_5 y_5^3+\alpha_5^2\beta_5^3\beta_6^3 k_5 y_5^3-8\beta_1^2\beta_2^2\beta_3^2\beta_4^2\beta_5^2\beta_6^2 y^2y_6-8\beta_1^2\beta_2^2\beta_3^2\beta_4^2\beta_5^2\beta_6^3 y^2y_6$$
$$+6\beta_1\beta_2\beta_3\beta_4\beta_5\beta_6 yy_6^2-6\beta_1\beta_2\beta_3\beta_4\beta_5\beta_6^3 yy_6^2+\beta_6 y_6^3+\beta_6^2 y_6^3-\beta_6^3 y_6^3-3\beta_6 k_6 y_6^3-3\beta_6^2 k_6 y_6^3-\beta_6^3 k_6 y_6^3\big)$$

APPENDIX B: DETAILED PROCESS DESCRIPTION OF NSDMA

Algorithm 1. Optimization algorithm of NSDMA[a]

Input: C_1, C_2, C_3, N_p, N_I, V_{min}, V_{max}
Output: Start point of six mirror system
Process:

```
Pop0 = GenerateIndivdual (V_min, V_max);
Pop0_m0 = a part of Pop0;
Pop0_f0 = a part of Pop0;
for Iter <= N_I do
    Pop0_m = Nondominated (Pop0_m0);
    Pop0_f = Nondominated (Pop0_f0);
    Temp = exp(−Iter/N_I);
    Q = C_1 exp((Iter − N_I)/N_I);
    if Q < 0.25 then
        Generate < Pop_m, Pop_f > via Eqs. (6), (8) in the
        literature [16];
    else
        if Temp > 0.6 then
            Generate < Pop_m, Pop_f > via Eq. (10)
            in the literature [16];
        else
            Generate < Pop_m, Pop_f > via Eqs. (11),
            (12), (15), (16) in the literature [16];
        endif
    endif
    Pop_m = Nondominated (Pop_m);
    Pop_f = Nondominated (Pop_f);
    PopI_m = Nondominated ([The top 50% of Pop0_m,
             The top 50% of Pop_m]);
    PopI_f = Nondominated ([The top 50% of Pop0_f,
             The top 50% of Pop_f]);
    Pop0_m0 = [The first 80% of PopI_m, GenerateIndividual
              (V_min, V_max) instead of the last 20% of PopI_m];
    Pop0_f0 = [The first 80% of PopI_f, GenerateIndividual
              (V_min, V_max) instead of the last 20% of PopI_f];
    Iter = Iter + 1;
endfor
```

N_p, N_I are the population size and the maximum number of iterations, respectively, and V_{min}, V_{max} are the minimum and maximum values that correspond to the 21 algorithm variables, respectively.

APPENDIX C: PRINCIPLE OF NONDOMINATED SORTING

Algorithm 2. Fast-Nondominated-Sort

Input: P
Output: H

```
for p ∈ P do
    for q ∈ P do
        if ∃(p < q) & ∀(p ≤ q) then
            S_p = S_p ∪ {q};
        elseif ∃(q < p) & ∀(q ≤ p) then
            n_p = n_p + 1;
        endif
    endfor
    if n_p = 0 then
        F_1 = F_1 ∪ p;
    endif
endfor
i = 1;
while F_i ≠ ∅ then
    H = ∅;
    for p ∈ F_i then
        for q ∈ S_p then
            n_p = n_p − 1;
            if n_p = 0 then
                H = H ∪ q;
            endif
        endfor
        i = i + 1; F_i = H;
    endfor
endwhile
```

(Table continued)

P contains the coordinate and fitness information of all individuals in the current iteration population, while H represents the ordered sequence of individuals in the population after being sorted by the algorithm, along with their corresponding coordinate and fitness information.

Funding. National Science and Technology Major Project (2018ZX02102002).

Disclosures. The authors declare no conflicts of interest.

Data availability. Data underlying the results presented in this paper are not publicly available at this time but may be obtained from the authors upon reasonable request.

REFERENCES

1. J. Chang, M. Zou, R. Wang, S. Feng, and M. M. Talha, "All-reflective optical system design for extreme ultraviolet lithography," Chin. Opt. Lett. **8**, 1082–1084 (2010).
2. X. Yan, Y. Li, Y. Li, L. Liu, and K. Liu, "Design of an extreme ultraviolet lithography projection objective with a grouping design method through forward and reverse real ray tracing," Appl. Opt. **61**, 7449–7454 (2022).
3. W. Tan, H. Ji, Y. Mo, and D. Ma, "Automatic design of an extreme ultraviolet lithography objective system based on the Seidel aberration theory," Appl. Opt. **61**, 8633–8640 (2022).
4. R. Flores-Hernandez, "AZTECA, a y-y diagram oriented interactive computer program for optical system design and optimization," Proc. SPIE **158**, 400–415 (1995).
5. S. A. Lerner, J. M. Sasian, and M. R. Descour, "Design approach and comparison of projection cameras for EUV lithography," Opt. Eng. **39**, 792–802 (2000).
6. O. E. Marinescu, "Novel design methods for high-quality lithographic objectives," Ph.D. thesis (West University of Timişoara, 2006).
7. C. Wang and D. L. Shealy, "Differential equation design of high-order aspheric surfaces," Proc. SPIE **5523**, 185–192 (2004).
8. C. Wang, "A differential equation design method for finite-conjugate, multi-mirror imaging systems," Ph.D. dissertation (The University of Alabama at Birmingham, 1992).
9. F. Liu and Y. Li, "Grouping design of eight-mirror projection objective for high-numerical aperture EUV lithography," Appl. Opt. **52**, 7137–7144 (2013).
10. Y. Wu, L. Wang, J. Yu, B. Yu, and C. Jin, "Design method for off-axis aspheric reflective optical system with extremely low aberration and large field of view," Appl. Opt. **59**, 10185–10193 (2020).
11. R. Hudyma, H.-J. Mann, and U. Dinger, "Projection system for EUV lithography," U.S. patentUS7375798 B2 (April 8, 2008).
12. L. I. U. Jun, W. Huang, and F. Hongjie, "A novel method for finding the initial structure parameters of optical systems via a genetic algorithm," Opt. Commun. **361**, 28–35 (2016).
13. W. Qiang, H. Y. Hu, W. M. He, L. W. Yue, Z. Qiang, D. X. Yang, Y. Huang, and Y. L. Li, *Photolithography Process Near the Diffraction Limit* (2020), p. 157.

14. N. Srinivas and K. Deb, "Multiobjective function optimization using nondominated sorting genetic algorithms," Evol. Comput. **2**, 221–1308 (1994).
15. K. Deb, S. Agrawal, A. Pratap, and T. Meyarivan, "A fast elitist non-dominated sorting genetic algorithm for multi-objective optimization: NSGA-II," in *International Conference on Parallel Problem Solving from Nature* (2000).
16. F. A. Hashim and A. G. Hussien, "Snake optimizer: a novel meta-heuristic optimization algorithm," Knowl. Based Syst. **242**, 108320 (2022).